Journal of Materials Chemistry A

PAPER

View Article Online
View Journal | View Issue



Cite this: J. Mater. Chem. A, 2015, 3, 7361

# A stable metal–organic framework with suitable pore sizes and rich uncoordinated nitrogen atoms on the internal surface of micropores for highly efficient $CO_2$ capture†

Shao-Juan Bao,[a] Rajamani Krishna,[c] Ya-Bing He,[d] Jun-Sheng Qin,[a] Zhong-Min Su,*[a] Shun-Li Li,[a] Wei Xie,[a] Dong-Ying Du,*[a] Wen-Wen He,[a] Shu-Ran Zhang[a] and Ya-Qian Lan*[ab]

Received 14th January 2015
Accepted 30th January 2015

DOI: 10.1039/c5ta00256g

www.rsc.org/MaterialsA

An air-stable tetrazolate-containing framework, $[Zn_2L_2]\cdot 2DMF$ (**NENU-520**, $H_2L$ = 4-(1*H*-tetrazole-5-yl) biphenyl-4-carboxylic acid), with uncoordinated N atoms on its internal surface was solvothermally synthesized and structurally characterized. This metal–organic framework (MOF) exhibited high $CO_2$ uptake of 79.9 $cm^3$ $cm^{-3}$ at 298 K and 100 kPa, as well as excellent adsorption selectivity for $CO_2$ over $CH_4$ and $N_2$. Particularly, its exceptionally high selectivity of $CO_2$ over $N_2$ at 298 K has ranked **NENU-520** among the highest MOFs for selective $CO_2$ separation. Furthermore, the potential application of **NENU-520** for the fixed bed pressure swing adsorption (PSA) separation of $CO_2$ from $CH_4$ and $N_2$ has been validated *via* simulated breakthrough experiments. The small channel with the size of 3.6 Å, combined with $CO_2$-accessible free nitrogen atoms directed toward the inner surface, is believed to contribute to its high $CO_2$ uptake capacity and selectivity. Thus, this work represents a unique way to target MOF materials for highly selective $CO_2$ separation by incorporating $CO_2$-philic functional sites on pore surfaces, and at the same time optimizing pore sizes.

## Introduction

Carbon dioxide ($CO_2$) emissions, which are inevitable, are mainly generated from the anthropogenic combustion of coal, oil and natural gas, the main energy resources for our daily life, economic growth and industrial development.[1–5] With the growing increase in the amount of $CO_2$ in the atmosphere, the undesirable global warming and climate change have attracted increasing attention.[6–10] Moreover, in addition to its involvement in the greenhouse effect, $CO_2$ is also highly associated with many issues such as the separation of $CO_2$ from industrial gas for bioremediation, demand of selectively captured $CO_2$ from methane in biogas streams and post-combustion flue gases generated from coal-fired power stations.[11–13] Consequently, there is still an urgent need to selectively capture and sequestrate $CO_2$ to reduce its negative effect in the atmosphere. Two points must first be made with regards to captured materials and their long-term usage. Firstly, they should be highly air-stable and be able to maintain their stability over multiple cycles for practical applications as functional materials.[14,15] Secondly, as a promising adsorbent for practical applications, they should possess not only good adsorption capacity but also high selectivity.[16–18] Adsorption capacity depends on the equilibrium pressure and temperature, the nature of the adsorbate, and the nature of the micropores in the adsorbent. To a great extent, the selective capture of $CO_2$ is related to the nature of the adsorbent in addition to the operational temperature and pressure.

Due to their high surface areas, high void volumes and controlled pore sizes, metal–organic frameworks (MOFs) represent a rapidly expanding, probable new class of porous adsorbents with a large range of possibilities for the design of functional materials.[19–22] The focus on exploiting their high surface areas and large pore size conventionally are far from enough. To date, various feasibility strategies, such as the introduction of a high density of open metal sites, charged skeleton of MOFs, and decoration with polar substituent groups

[a]Institute of Functional Material Chemistry, Faculty of Chemistry, Northeast Normal University, Changchun 130024, Jilin, P. R. China. E-mail: zmsu@nenu.edu.cn
[b]Jiangsu Key Laboratory of Biofunctional Materials, School of Chemistry and Materials Science, Nanjing Normal University, Nanjing 210023, Jiangsu, P. R. China. E-mail: yqlan@njnu.edu.cn
[c]Van't Hoff Institute for Molecular Sciences, University of Amsterdam Science Park 904, 1098 XH Amsterdam, The Netherlands
[d]College of Chemistry and Life Sciences, Zhejiang Normal University, Jinhua 321004, Zhejiang, China

† Electronic supplementary information (ESI) available: Experimental details, PXRD patterns, TGA, IR curves, crystallographic data, additional figures, IAST and breakthrough calculations for **NENU-520**. CCDC 990058. For ESI and crystallographic data in CIF or other electronic format see DOI: 10.1039/c5ta00256g

(for instance, –COOH, $–NH_2$, –OH), have been explored to enforce their interactions and thus enhance the adsorption capacity and selectivity of MOFs toward $CO_2$.[23–27] Moreover, given the fact that the kinetic diameters of the cylinders are 3.3 Å, 3.64 Å and 3.80 Å for $CO_2$, $N_2$ and $CH_4$, respectively, size selectivity is an attractive characteristic for $CO_2$ separation and capture.[28,29] To effectively realize $CO_2$ separation on the basis of size, precise control of the limiting pore diameter is of significant importance. The study of $CO_2$ selectivity based on small pore size is numbered, albeit more and more MOFs have been reported.

A straightforward approach was put forward and tested by the groups of Chen, Bu, Zhao and Su.[30–33] The introduction of abundant uncoordinated nitrogen atoms may produce a stronger interaction with $CO_2$. Typically, the interaction between the localized dipoles of a N-containing group and the quadrupole moment of $CO_2$ could induce dispersion and electrostatic forces to enhance the $CO_2$ adsorption and separation abilities of MOFs. Nevertheless, a high percentage of N-donor sites is not always beneficial to further enhance the interaction with $CO_2$ molecules. For example, when the lone electron pairs of partially exposed nitrogen atoms do not point into the channels of the frameworks or the uncoordinated N-donor sites are blocked by functionalized groups, they have a lower effect on the improvement of the $CO_2$ capacity. It is of crucial importance to construct MOFs that effectively utilize the accessible nitrogen atoms from organic linkers.

Herein, we selected a tetrazolate-containing $H_2L$ (4-(1*H*-tetrazole-5-yl)biphenyl-4-carboxylic acid) as an organic linker to construct a new MOF. Fortunately, an air-stable zinc-based MOF, $[Zn_2L_2]\cdot 2DMF$ (**NENU-520**, **NENU** = Northeast Normal University) was successfully synthesized and the inner surface is polarized with uncoordinated nitrogen atoms. It features a small channel (3.6 Å, which is slightly larger than the kinetic diameter of $CO_2$), which is favourable for its potential application in gas capture and separation. As anticipated, an activated sample **NENU-520a** exhibits a high uptake of $CO_2$ and $H_2$ with high isosteric heat. Its selectivities for $CO_2/CH_4$ and $CO_2/N_2$ were evaluated using the ideal adsorbed solution theory (IAST) and simulated breakthrough experiments. Remarkably, the results from these studies all confirm that the selectivity of $CO_2/N_2$ has featured **NENU-520** among the highest porous MOFs for $CO_2$ selective separation under ambient conditions. **NENU-520** is one of the best materials to facilitate effective $CO_2$ separation and capture.

## Results and discussion

**NENU-520** was synthesized by the solvothermal reaction of $Zn(NO_3)_2\cdot 6H_2O$ and $H_2L$ in a solvent mixture of DMF–EtOH with the addition of a small amount of $HNO_3$ at 90 °C for 3 days. The highly crystallized **NENU-520** was formulated as $[Zn_2L_2]\cdot 2DMF$ on the basis of the single-crystal X-ray diffraction study. The X-ray crystallographic analysis reveals that **NENU-520** crystallizes in the monoclinic space group *Cc* (Table S1†). The asymmetric unit consists of two independent Zn(II) atoms, one coordinated DMF molecule, one DMF solvent and two distinct

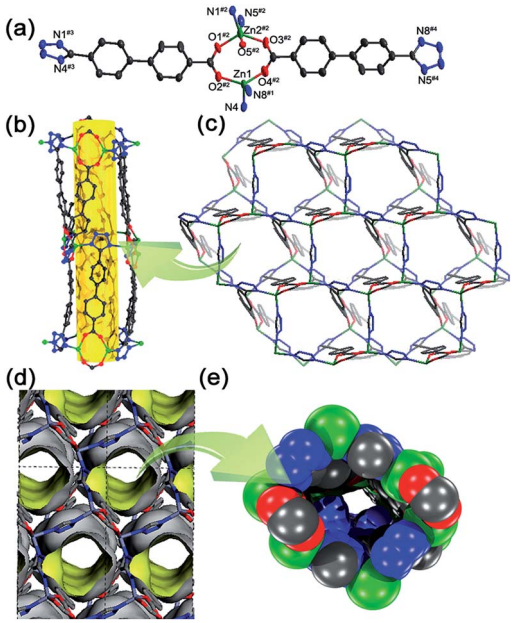


Fig. 1 The structure of **NENU-520**: (a) the coordination environments of Zn(II) atoms, symmetry codes: #1 0.5 + *x*, 0.5 + *y*, *z*; #2 1 + *x*, *y*, *z*; #3 0.5 + *x*, 1.5 − *y*, 0.5 + *z*; #4 *x*, 1 − *y*, −0.5 + *z*; (b) the 1D channel along the *b* axis; (c) 3D framework of **NENU-520** along the *c* axis; (d) the Connolly surface diagram displays the three dimensional irregular tunnels of **NENU-520**, and (e) the 1D channel in spacefilling mode along the *c* axis. All the hydrogen atoms are omitted for clarity.

$L^{2-}$ moieties (Fig. 1a). In **NENU-520**, Zn1 and Zn2 atoms are linked by carboxyl groups to form a binuclear zinc cluster, in addition, each tetrazolyl group bonds two independent Zn atoms from two zinc clusters. In **NENU-520**, each ligand uses just two N atoms for the framework formation, leaving two other open N-donor sites. Such interlinkage generates a 1D smaller-size curving channel running along the *b* axis with a size of ~3.6 Å (Fig. 1b and c). The Connolly surface diagram (Fig. 1d) displays the irregular channels of the framework structures. It is evident that the left two N atoms point to the inner surface (Fig. 1e). The overall framework can be designated as a (3, 3, 6)-connected network (Fig. S4a†) with the point symbol of $(4\cdot 6^2)_2(4^2\cdot 6^7\cdot 8^6)$ analyzed by the TOPOS program, if the $L^{2-}$ and binuclear zinc cluster are regarded as 3- and 6-connected nodes, respectively. Further close observation of the structure shows that **NENU-520** can be simplified as a (4, 4)-connected topology with the point symbol of $(4^2\cdot 6^6\cdot 8)$, when each Zn atom and $L^{2-}$ fragment is considered as a discrete 4-connected node (Fig. S3†). In addition, the phase purity of the bulk material was independently confirmed by powder X-ray diffraction (PXRD, Fig. S4b†). Upon removing DMF solvent molecules, **NENU-520** forms a microporous framework containing 27.4% solvent void accessible.[34] It is noteworthy that **NENU-520** shows good air-stability even when exposed to air for more than two weeks (Fig. S5†), which is of utmost importance for practical applications.[35,36]

The permanent porosity of **NENU-520** was unambiguously established by its $N_2$ sorption isotherm at 77 K. The activated sample **NENU-520a** was prepared by exchanging the solvent and

 

it was characterized by thermal gravimetric analysis (TGA, Fig. S6†) and PXRD patterns (Fig. S5†), indicating that the framework was maintained because the broadened peaks positions remained. **NENU-520a** shows a characteristic type I behaviour with a BET surface area of 387 $m^2\ g^{-1}$ and a pore volume of 0.27 $cm^3\ g^{-1}$ based on its $N_2$ sorption isotherm (Fig. 2). The slight hysteresis between the adsorption and desorption profile can perhaps be explained by the 1D narrow channel system, which hints the escape of adsorbed gas molecules, as well as probably involving the structural breathing of the framework during the adsorption–desorption process.[37,38] Using the Horvath–Kawazoe (HK) method on the $N_2$ desorption isotherms, pore size distribution (Fig. 2) was estimated, which is basically identical to the results from the single-crystal X-ray diffraction study.

Low-pressure $H_2$ adsorption isotherms for **NENU-520a** were collected at 77 and 87 K, which are completely reversible, as shown in Fig. S7a.† **NENU-520a** adsorbs 1.36 wt% of $H_2$ (152.4 $cm^3\ g^{-1}$ or 19.6 $H_2$ molecules per formula unit) at 77 K, and 1.09 wt% (121.6 $cm^3\ g^{-1}$ or 15.5 $H_2$ molecules per formula unit) at 87 K. It is indicative of the presence of strongly polarizing binding sites with a high affinity for $H_2$ from the steep initial portion of each isotherm. To gain further insight into $H_2$ adsorption, the behaviour of the isosteric heat was calculated using the Clausius–Clapeyron equation.[39] **NENU-520a** shows a near-zero coverage $Q_{st}$ value of 10.7 kJ $mol^{-1}$ (Fig. S7b†), which is comparable with many famous porous materials such as MOF-5 (7.6 kJ $mol^{-1}$), Zn–MOF-74 (8.3 kJ $mol^{-1}$), NOTT-101 (5.3 kJ $mol^{-1}$) and UMCM-150 (7.3 kJ $mol^{-1}$).[40,41] This result was attributed to the small pore diameter in **NENU-520a**, wherein overlapping potentials from two or more pore walls interact with a single $H_2$ molecule.[42,43] In addition, the uncoordinated N-heteroatom sites also aid in the low-pressure uptake by this material.[31]

Because accessible N-donor sites are expected to enhance interactions between frameworks and $CO_2$, the $CO_2$ sorption isotherms were measured at different temperatures, which shows a fully reversible type I behaviour with no hysteresis (Fig. 3). The $CO_2$ uptake of **NENU-520a** at saturation was 106.0 $cm^3\ cm^{-3}$ (corresponding to 15.7 wt% or 10.3 $CO_2$ per formula unit, Table S3†) at 273 K and 79.9 $cm^3\ cm^{-3}$ (corresponding to 11.9 wt% or 7.8 $CO_2$ per formula unit) at 298 K. Albeit these values are lower than the M–MOF-74 series (162 $cm^3\ cm^{-3}$) with different open metal sites, they are considerably higher than lots of well-known MOFs such as MAF-23 (or $Zn_2(btm)_2$, 74.2 $cm^3\ g^{-1}$ and 56.1 $cm^3\ g^{-1}$ at 273 K and 298 K) with multiple strong adsorption sites and $[Cu(tba)_2]_n$ (51.8 $cm^3\ g^{-1}$ or 10.2 wt% at 273 K), the currently best performing ZIF-69 (70 $cm^3\ g^{-1}$ at 273 K and 1 atm).[44–46] For the practical use of an adsorptive material, its regeneration and recycling properties are crucial and are also important standards to evaluate an adsorption material. Keeping this in mind, the regenerative feature of **NENU-520a** was investigated. The powder X-ray diffraction pattern (Fig. S8†) of **NENU-520a** after three cycles is in good agreement with that of its original structural characteristics, revealing its good stability. Moreover, **NENU-520a** basically maintains high adsorption capacity after three cycles of the regeneration experiment. This excellent behavior is significant for all of the MOFs analyzed, and the reproducibility demonstrates that uptake and release is nondestructive.

The sorption behaviours of **NENU-520a** toward $CH_4$ and $N_2$ were also studied at 273 and 298 K (Fig. 3). The desolvated **NENU-520a** only has a maximum $CH_4$ uptake of 31.3 $cm^3\ g^{-1}$ (1.4 mmol $g^{-1}$, 2.24 wt%) and 21.41 $cm^3\ g^{-1}$ (0.96 mmol $g^{-1}$, 1.53 wt%) at 273 and 298 K, respectively, which is substantially lower than $CO_2$. In sharp contrast to $CO_2$ and $CH_4$, the uptake of $N_2$ reaches a maximum of only 6.6 $cm^3\ g^{-1}$ (0.29 mmol $g^{-1}$) at

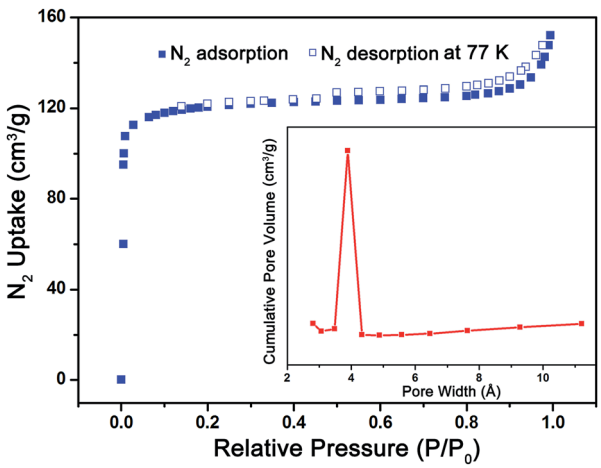


Fig. 2 The $N_2$ sorption isotherms at 77 K. Inset: the pore size distribution of **NENU-520a** using the Horvath–Kawazoe (HK) method.

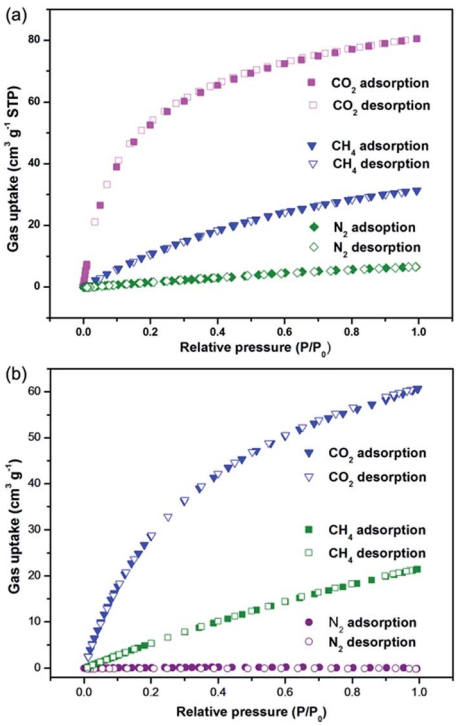


Fig. 3 The $CO_2$, $CH_4$ and $N_2$ sorption isotherms for **NENU-520a** at 273 K (a) and 298 K (b), respectively.

273 K and 0.23 $cm^3\ g^{-1}$ (0.01 mmol $g^{-1}$) at 298 K, respectively. It is clearly shown that the pore structure of **NENU-520a** is readily accessible to $CO_2$. The relatively high $CO_2$ and marginal $N_2$ uptake at ambient temperature prompted us to investigate the capacity of **NENU-520a** to selectively adsorb $CO_2$ over $CH_4$ and $N_2$.

The ideal adsorbed solution theory (IAST) calculation, which originated from Myers and Prausnitz,[47] was employed to predict the adsorption selectivity and $CO_2$ uptake of **NENU-520a** for the following binary gas mixtures: 15/85 $CO_2/N_2$, 50/50 $CO_2/CH_4$ and 5/95 $CO_2/CH_4$. The Langmuir–Freundlich equation fits extremely well with the single-component isotherms at 273 and 298 K (Fig. S9†), and the fitting parameters are listed in Table S4.† The evaluation of the selectivity of adsorbents at atmospheric pressure for the $CO_2$–$N_2$ mixture was essential for a realistic post-combustion capture of $CO_2$. In these calculations, the partial pressures of $CO_2$ and $N_2$ are taken to be 15 kPa and 85 kPa, respectively. For comparison, six representative MOFs or zeolites (NaX, MgMOF-74, Cu–TDPAT, UTSA-16, Cu–SSZ13 and ZnMOF-74)[35,36] exhibiting high $CO_2/N_2$ separation selectivity are also included. Fig. 4 presents the IAST calculations for $CO_2/N_2$ adsorption selectivity. Remarkably, **NENU-520** has the highest selectivity (about 400) towards $CO_2$ for the mixture compositions. To the best of our knowledge, only two MOFs were reported to display higher $CO_2/N_2$ selectivity than **NENU-520**. One example is SIFSIX-3–Zn, which exhibits the highest $CO_2/N_2$ selectivity (with selectivity of 1539 ± 307).[28] During the course of this work, SIFSIX-3–Zn had more-regular square-shaped channels with a dimension of 3.84 Å and was lined with Lewis basic groups on the $SiF_6$ anions which notably enhance the uptake of $CO_2$ into the material, whereas neither charged units nor favourable groups exist in the channels of **NENU-520**. The other MOF is [Cu(bcppm)$H_2O$]. Although [Cu(bcppm)$H_2O$] has slightly higher selectivity, its uptake capacity (1.70 and 1.85 mmol $g^{-1}$ at 293 and 273 K, respectively) is apparently lower than **NENU-520** (2.71 and 3.59 mmol $g^{-1}$ at 298 and 273 K, respectively).[36] Its selectivity is evidently superior to most MOFs and this ranks **NENU-520** among the highest selectivity values (Table S5†) with the absence of unsaturated metal centres, charged units and amine groups.[46,48–57] Thus, **NENU-520** is one of the best materials to facilitate effective $CO_2$ capture and separation from the perspective of comprehensive properties.

The selectivities for $CO_2/CH_4$ were also evaluated when the gas phase compositions were 5/95 and 50/50 (Fig. S10†), and the corresponding values are comparable to most MOFs reported in the literature, although it has a lower selectivity than Mg–MOF-74.

In view of the feasibility of the separation performance of **NENU-520**, transient breakthrough simulations using the methodology described in the literature was performed.[58–64] The performance of industrial fixed bed adsorbers is dictated by a combination of adsorption selectivity and uptake capacity. The proper combination of both of these factors is obtained by the use of breakthrough calculations. Fig. 5a shows a schematic of a packed bed adsorber. The $x$ axis in Fig. 5b and c is dimensionless time, $\tau$, which is defined by dividing the actual time, $t$, by the characteristic times, $L\varepsilon/u$. A longer breakthrough time is desirable from a practical point of view because this indicates a less frequent requirement for regeneration. Fig. 5b presents the breakthrough characteristic as a function of the dimensionless time in an adsorber packed with **NENU-520a** at a total pressure of 100 kPa for a 15/85 $CO_2/N_2$ mixture, which represents the conditions relevant for flue gas processing. For **NENU-520a**, the sequence of breakthroughs is dictated by its adsorption strength and the more strongly adsorbing $CO_2$ elutes last in the sequence. Fig. 5c presents the mole percent of $N_2$ in outlet gas as a function of dimensionless time with **NENU-520a**. It is possible to recover pure $N_2$ from the gas mixture in a certain interval of time. We arbitrarily set the purity requirement to be 99.95% $N_2$. This amount can be determined from a material balance. The productivity of $N_2$ with a purity of 99.95%+ was determined to be 4.84 mol $kg^{-1}$ of **NENU-520**. The reason for

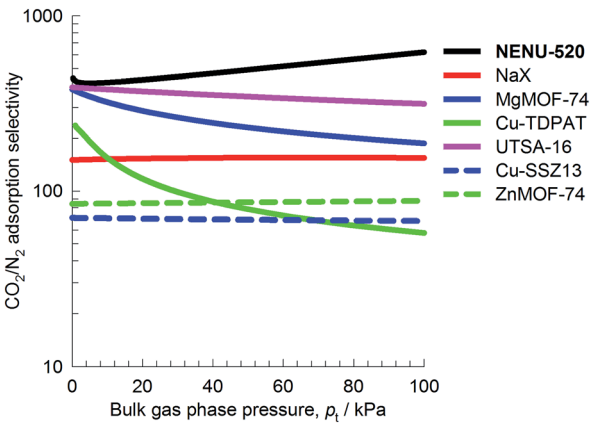


Fig. 4 Calculated selectivity of $CO_2/N_2$ predicted by IAST calculations 298 K for the variety of MOFs considered in this work. In these calculations, the partial pressures of $CO_2$ and $CH_4$ are taken to be $p_1/p_2$ = 15/85.

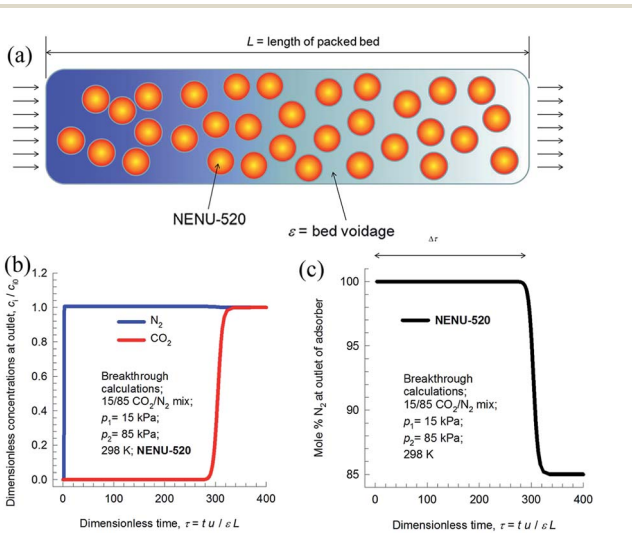


Fig. 5 (a) Schematic view of a packed bed adsorber. The tube length $L$ = 0.3 m. The apparatus was operated at 298 K. The bed porosity, $\varepsilon$ = 0.4. The interstitial gas velocity, $u$ = 0.04 m $s^{-1}$; (b) breakthrough characteristics of an adsorber packed with **NENU-520** and maintained at isothermal conditions at 298 K, and (c) mole percent $N_2$ in outlet gas as a function of dimensionless time for operation at a total pressure of 100 kPa for 15/85 $CO_2/N_2$ mixture.

the high productivity is a combination of higher selectivity and higher $CO_2$ uptake capacity. **NENU-520a** was demonstrated to be a promising candidate for $CO_2$ capture and separation from fuel gas.

5/95 $CO_2/CH_4$ mixture breakthrough characteristics as a function of dimensionless time were measured in an adsorber packed with **NENU-520** (as shown in Fig. S11†). **NENU-520** outperforms ZIF-78 (81), UTSA-20a (86), MIL-101 (32) and many others by having a longer breakthrough time.[28] In natural gas purification processes, the primary objective is to produce $CH_4$ with a specified purity level, which is typically 500 ppm $CO_2$, *i.e.* 0.05 mole percent $CO_2$. Fig. S11b† shows the gas composition, expressed as mole percent of $CH_4$, in outlet gas as a function of dimensionless time for a selection of porous adsorbent materials. During the time interval $\Delta\tau$, 99.95% + pure $CH_4$ can be produced. The productivity of methane with a purity of 99.95%+ is calculated to be 6.7 mol $kg^{-1}$ of **NENU-520**, which was determined from the material balance on the fixed bed adsorber. In addition, the composition of natural gas changes frequently. The breakthrough characteristics for a binary 50/50 mixture of $CO_2$ and $CH_4$ are also presented (Fig. S12†). The breakthrough occurs at a shorter dimensionless time than for the 5/95 binary mixture. And the productivity is 1.79 mol per kg of **NENU-520** during the time interval $\Delta\tau$. The results from all these studies confirm that **NENU-520** has the ability to separate $N_2$ and $CH_4$ in the pure form from gas mixtures. Based on the presented evidence, **NENU-520** is a superior adsorbent for $CO_2/N_2$ and $CO_2/CH_4$ separation at ambient conditions than reported for most of the MOFs.

The $CO_2$ adsorption enthalpy of **NENU-520a** is 33 kJ $mol^{-1}$ (Fig. 6), which is stronger than siliceous zeolite (27 kJ $mol^{-1}$), and the series of MAF materials (MAF-4, 25.1 kJ $mol^{-1}$; MAF-7, 17.2 kJ $mol^{-1}$; MAF-25, 26.3 kJ $mol^{-1}$ and MAF-26, 23.3 kJ $mol^{-1}$; MAF stands for metal azolate framework).[30,65,66] Its $CH_4$ adsorption enthalpy is 29 kJ $mol^{-1}$. The high uptake and enthalpy of $CO_2$ as well as the remarkable selectivity over $CH_4$ and $N_2$ may be reasonable considering the fact that: (i) with its greater polarizability and larger quadrupole moment, $CO_2$ has stronger interactions with the accessible N-sites of **NENU-520** than $CH_4$ and $N_2$;[67–69] (ii) the abundant uncoordinated N-heteroatom sites directed toward the inner surface in the narrow cavities are beneficial to interact with $CO_2$ molecules; (iii) as mentioned above, the kinetic diameters of the cylinders are 3.3 Å, 3.64 Å and 3.80 Å for $CO_2$, $N_2$ and $CH_4$, respectively. The limiting pore size (about 3.6 Å) of **NENU-520** is just right for $CO_2$. Thus, $CO_2$ molecules are more prone to be injected than $CH_4$ and $N_2$.

Inspired by the reported charge transfer electron transitions between microporous MOFs and guest molecules, the potential luminescent sensitivity and selectivity of **NENU-520** were also investigated in different organic solvents such as cyclohexane, toluene, acetonitrile, benzene, chloroform, *p*-xylene, *n*-hexane, *m*-xylene, THF and nitrobenzene. The results suggest that the emission intensities are largely dependent on different solvent molecules (Fig. S13a and b†). Moreover, the evident quenching phenomenon for nitrobenzene was examined in detail (see ESI†). As shown in Fig. S13c and d,† **NENU-520** can sensitively detect a very small amount of nitrobenzene (30 ppm in DMF) through noticeable fluorescence decay, demonstrating extremely high sensitivity towards nitrobenzene. To date, several MOF-based fluorescent sensors have been developed for the detection of nitroaromatic explosives.[70,71] The intensity of **NENU-520** was nearly completely quenched at a concentration of 100 ppm with a high quenching efficiency of 96.6%, which is higher than other MOF sensors toward nitrobenzene.[72] In addition, **NENU-520** can be regenerated for recycling by centrifuging the solution after use and then washing several times with DMF. The quenching efficiencies of cycle 1–4 did not decrease (100 ppm), displaying its high recyclability and stability in detection applications (Fig. S14, S15 and S16†), which is favourable for its potential application in detecting explosives containing nitrobenzene molecules. Referring to the reported works of Sun[71] and Zhang[72], **NENU-520** is presumably attributed to not only the good dispersible nature of its MOF particles but also to the electron deficient nature of nitrobenzene and the high electron rich conjugated framework structure.[70,71]

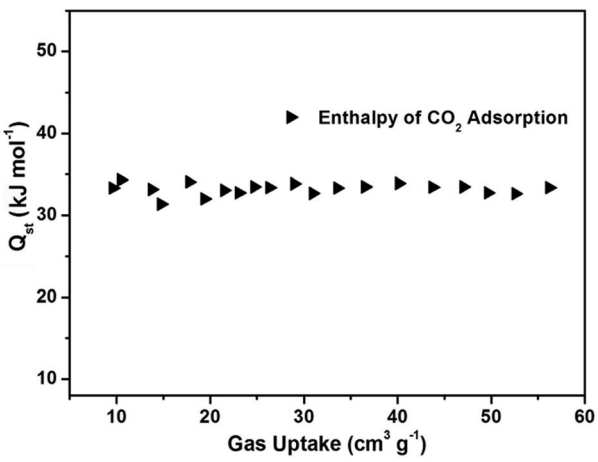


Fig. 6 Heats of $CO_2$ adsorption as a function of $CO_2$ uptake for NENU-520.

## Conclusions

In conclusion, a new N-rich MOF has been successfully synthesized by means of a solvothermal reaction. **NENU-520** has good air-stability even in the presence of moisture. Activated **NENU-520a** exhibits a strong adsorption capacity towards $H_2$ and $CO_2$ with the high adsorption enthalpy of 10.7 kJ $mol^{-1}$ and 33 kJ $mol^{-1}$, respectively. Moreover, **NENU-520a** shows high $CO_2/CH_4$ and $CO_2/N_2$ selectivities, which were calculated *via* a combination of the ideal adsorbed solution theory and breakthrough simulations for a realistic consideration. In particular, the selectivity of $CO_2$ over $N_2$ at 298 K of **NENU-520a** is amongst the highest values for $CO_2$ selective separation. Consequently, **NENU-520a** has significant potential for use as an adsorbent in $CO_2$-capture for natural gas sweetening and post-combustion power plants, by combining the higher uptake and higher selectivity toward $CO_2$. Its narrow but suitable channel as well as

effective accessible nitrogen donors directed toward the inner surface is demonstrated to be the predominant factors for its high uptake capacity and unprecedented selectivity. In addition, **NENU-520a** displays highly selective, sensitive and recyclable properties in the detection of nitrobenzene as a fluorescent sensor because of its quenching effect on nitrobenzene.

## Acknowledgements

This work was financially supported by Pre-973 Program (no. 2010CB635114), the National Natural Science Foundation of China (no. 21371099, 21471080 and 21401021), China Postdoctoral Science Foundation (no. 2014M551154), the Science and Technology Development Planning of Jilin Province (no. 20140203006GX and 20140520089JH), the Fundamental Research Funds for the Central Universities (no. 14QNJJ013), the Jiangsu Specially-Appointed Professor, the NSF of Jiangsu Province of China (no. BK20130043), the Natural Science Research of Jiangsu Higher Education Institutions of China (no. 13KJB150021), the Priority Academic Program Development of Jiangsu Higher Education Institutions and the Foundation of Jiangsu Collaborative Innovation Center of Biomedical Functional Materials.

## Notes and references

1 J. R. Li, J. Sculley and H. C. Zhou, *Chem. Rev.*, 2012, **112**, 869.
2 D. M. D'Alessandro, B. Smit and J. R. Long, *Angew. Chem., Int. Ed.*, 2010, **49**, 6058.
3 M. Z. Jacobson, *Energy Environ. Sci.*, 2009, **2**, 148.
4 K. M. K. Yu, I. Curcic, J. Gabriel and S. C. E. Tsang, *ChemSusChem*, 2008, **1**, 893.
5 G. Petron, P. Tans, G. Frost, D. Chao and M. Trainer, *J. Geophys. Res.*, 2008, **113**, 1.
6 S. Solomon, G. K. Plattnera, R. Knutti and P. Friedlingstein, *Proc. Natl. Acad. Sci. U. S. A.*, 2009, **106**, 1704.
7 N. MacDowell, N. Florin, A. Buchard, J. Hallett, A. Galindo, G. Jackson, C. S. Adjiman, C. K. Williams, N. Shah and P. Fennell, *Energy Environ. Sci.*, 2010, **3**, 1645.
8 E. D. Bloch, L. J. Murray, W. L. Queen, S. Chavan, S. N. Maximoff, J. P. Bigi, R. Krishna, V. K. Peterson, F. Grandjean, G. J. Long, B. Smit, S. Bordiga, C. M. Brown and J. R. Long, *J. Am. Chem. Soc.*, 2011, **133**, 14814.
9 S. Chaemchuen, N. A. Kabir, K. Zhou and F. Verpoort, *Chem. Soc. Rev.*, 2013, **42**, 9304.
10 J. Wang, L. Huang, R. Yang, Z. Zhang, J. Wu, Y. Gao, Q. Wang, D. O'Hare and Z. Zhong, *Energy Environ. Sci.*, 2014, **7**, 3478.
11 R. Service, *Science*, 2004, **305**, 962.
12 B. A. Peppley, *Int. J. Green Energy*, 2006, **3**, 195.
13 N. Muradov, *Int. J. Hydrogen Energy*, 2001, **26**, 1165.
14 H.-L. Jiang, D. Feng, K. Wang, Z.-Y. Gu, Z. Wei, Y.-P. Chen and H.-C. Zhou, *J. Am. Chem. Soc.*, 2013, **135**, 13934.
15 Z. Yin, Q. X. Wang and M. H. Zeng, *J. Am. Chem. Soc.*, 2012, **134**, 4857.
16 Y. He, W. Zhou, R. Krishna and B. Chen, *Chem. Commun.*, 2012, **48**, 11813.
17 Y. Q. Lan, H. L. Jiang, S. L. Li and Q. Xu, *Adv. Mater.*, 2011, **23**, 5015.
18 F. Akhtar, Q. Liu, N. Hedin and L. Bergström, *Energy Environ. Sci.*, 2012, **5**, 7664.
19 J. B. DeCoste and G. W. Peterson, *Chem. Rev.*, 2014, **114**, 5727.
20 Y. He, B. Li, M. O'Keeffe and B. Chen, *Chem. Soc. Rev.*, 2014, **43**, 5618.
21 Z. Zhang, Y. Zhao, Q. Gong, Z. Li and J. Li, *Chem. Commun.*, 2013, **49**, 653.
22 J. R. Li, R. J. Kuppler and H. C. Zhou, *Chem. Soc. Rev.*, 2009, **38**, 1477.
23 S. Couck, J. F. M. Denayer, G. V. Baron, T. Remy, J. Gascon and F. Kapteijn, *J. Am. Chem. Soc.*, 2009, **131**, 6326.
24 R. Vaidhyanathan, S. S. Iremonger, G. K. H. Shimizu, P. G. Boyd, S. Alavi and T. K. Woo, *Angew. Chem., Int. Ed.*, 2012, **51**, 1826.
25 J. L. C. Rowsell and O. M. Yaghi, *Angew. Chem., Int. Ed.*, 2005, **44**, 4670.
26 B. Zheng, Z. Yang, J. Bai, Y. Li and S. Li, *Chem. Commun.*, 2012, **48**, 7025.
27 Y. Wang, C. Tan, Z. Sun, Z. Xue, Q. Zhu, C. Shen, Y. Wen, S. Hu, Y. Wang, T. Sheng and X. Wu, *Chem.–Eur. J.*, 2014, **20**, 1341.
28 P. Nugent, Y. Belmabkhout, S. D. Burd, A. J. Cairns, R. Luebke, K. Forrest, T. Pham, S. Ma, B. Space, L. Wojtas, M. Eddaoudi and M. J. Zaworotko, *Nature*, 2013, **495**, 80.
29 J. M. Taylor, K. W. Dawson and G. K. H. Shimizu, *J. Am. Chem. Soc.*, 2013, **135**, 1193.
30 J. B. Lin, J. P. Zhang and X. M. Chen, *J. Am. Chem. Soc.*, 2010, **132**, 6654.
31 J. S. Qin, D. Y. Du, W. L. Li, J. P. Zhang, S. L. Li, Z. M. Su, X. L. Wang, Q. Xu, K. Z. Shao and Y. Q. Lan, *Chem. Sci.*, 2012, **3**, 2114.
32 P. Cui, Y. G. Ma, H. H. Li, B. Zhao, J. R. Li, P. Cheng, P. B. Balbuena and H. C. Zhou, *J. Am. Chem. Soc.*, 2012, **134**, 18892.
33 Q. Lin, T. Wu, S. T. Zheng, X. Bu and P. Feng, *J. Am. Chem. Soc.*, 2012, **134**, 784.
34 A. L. Spek, *J. Appl. Crystallogr.*, 2003, **36**, 7.
35 S. Xiang, Y. He, Z. Zhang, H. Wu, W. Zhou, R. Krishna and B. Chen, *Nat. Commun.*, 2012, **3**, 954.
36 W. M. Bloch, R. Babarao, M. R. Hill, C. J. Doonan and C. J. Sumby, *J. Am. Chem. Soc.*, 2013, **135**, 10441.
37 S. Xiang, J. Huang, L. Li, J. Zhang, L. Jiang, X. J. Kuang and C.-Y. Su, *Inorg. Chem.*, 2011, **50**, 1743.
38 L. Hou, L. N. Jia, W. J. Shi, Y. Y. Wang, B. Liu and Q. Z. Shi, *Dalton Trans.*, 2013, **42**, 3653.
39 S. S. Kaye and J. R. Long, *J. Am. Chem. Soc.*, 2005, **127**, 6506.
40 M. P. Suh, H. J. Park, T. K. Prasad and D. W. Lim, *Chem. Rev.*, 2012, **112**, 782.
41 R. B. Lin, D. Chen, Y. Y. Lin, J. P. Zhang and X. M. Chen, *Inorg. Chem.*, 2012, **51**, 9950.
42 M. Dincă, A. Dailly, Y. Liu, C. M. Brown, D. A. Neumann and J. R. Long, *J. Am. Chem. Soc.*, 2006, **128**, 16876.

 

43 S. L. Li and Q. Xu, *Energy Environ. Sci.*, 2013, **6**, 1656.
44 J. Duan, M. Higuchi, R. Krishna, T. Kiyonaga, Y. Tsutsumi, Y. Sato, Y. Kubota, M. Takata and S. Kitagawa, *Chem. Sci.*, 2014, **5**, 660.
45 P. Q. Liao, D. D. Zhou, A. X. Zhu, L. Jiang, R. B. Lin, J. P. Zhang and X. M. Chen, *J. Am. Chem. Soc.*, 2012, **134**, 17380.
46 M. Du, C. P. Li, M. Chen, Z. W. Ge, X. Wang, L. Wang and C. S. Liu, *J. Am. Chem. Soc.*, 2014, **136**, 10906.
47 A. L. Myers and J. M. Prausnitz, *AIChE J.*, 1965, **11**, 121.
48 B. Zheng, J. Bai, J. Duan, L. Wojtas and M. J. Zaworotko, *J. Am. Chem. Soc.*, 2011, **133**, 748.
49 M. Zhang, Q. Wang, Z. Lu, H. Liu, W. Liu and J. Bai, *CrystEngComm*, 2014, **16**, 6287.
50 A. K. Sekizkardes, T. İslamoğlu, Z. Kahveci and H. M. El-Kaderi, *J. Mater. Chem. A*, 2014, **2**, 12492.
51 T. M. McDonald, W. R. Lee, J. A. Mason, B. M. Wiers, C. S. Hong and J. R. Long, *J. Am. Chem. Soc.*, 2012, **134**, 7056.
52 X. Lv, L. Li, S. Tang, C. Wang and X. Zhao, *Chem. Commun.*, 2014, **50**, 6886.
53 Y. Liu, S. Wu, G. Wang, G. Yu, J. Guan, C. Pan and Z. Wang, *J. Mater. Chem. A*, 2014, **2**, 7795.
54 R.-J. Li, M. Li, X.-P. Zhou, S. W. Ng, M. O'Keeffe and D. Li, *CrystEngComm*, 2014, **16**, 6291.
55 L. Du, Z. Lu, K. Zheng, J. Wang, X. Zheng, Y. Pan, X. You and J. Bai, *J. Am. Chem. Soc.*, 2013, **135**, 562.
56 J. B. Lin and G. K. H. Shimizu, *Inorg. Chem. Front.*, 2014, **1**, 302.
57 T. M. McDonald, D. M. D'Alessandro, R. Krishna and J. R. Long, *Chem. Sci.*, 2011, **2**, 2022.
58 R. Krishna and J. R. Long, *J. Phys. Chem. C*, 2011, **115**, 12941.
59 R. Krishna, *Microporous Mesoporous Mater.*, 2014, **185**, 30.
60 D. L. Chen, H. Shang, W. Zhu and R. Krishna, *Chem. Eng. Sci.*, 2014, **117**, 407.
61 D. L. Chen, N. Wang, F. F. Wang, J. Xie, Y. Zhong, W. Zhu, J. K. Johnson and R. Krishna, *J. Phys. Chem. C*, 2014, **118**, 17831.
62 H. H. Wu, K. X. Yao, Y. H. Zhu, B. Y. Li, Z. Shi, R. Krishna and J. Li, *J. Phys. Chem. C*, 2012, **116**, 16609.
63 C. Song, Y. He, B. Li, Y. Ling, H. Wang, Y. Feng, R. Krishna and B. Chen, *Chem. Commun.*, 2014, **50**, 12105.
64 J. J. Perry, S. L. TeichMcGoldrick, S. T. Meek, J. A. Greathouse, M. Haranczyk and M. D. Allendorf, *J. Phys. Chem. C*, 2014, **118**, 11685.
65 Z. Zhang, Z. Z. Yao, S. Xiang and B. Chen, *Energy Environ. Sci.*, 2014, **7**, 2868.
66 R. Dawson, E. Stockel, J. R. Holst, D. J. Adams and A. I. Cooper, *Energy Environ. Sci.*, 2011, **4**, 4239.
67 K. Sumida, D. L. Rogow, J. A. Mason, T. M. McDonald, E. D. Bloch, Z. R. Herm, T.-H. Bae and J. R. Long, *Chem. Rev.*, 2012, **112**, 724.
68 Y.-S. Bae and C. H. Lee, *Carbon*, 2005, **43**, 95.
69 S. R. Caskey, A. G. Wong-Foy and A. J. Matzger, *J. Am. Chem. Soc.*, 2008, **130**, 10870.
70 H. Xu, F. Liu, Y. Cui, B. Chen and G. Qian, *Chem. Commun.*, 2011, **47**, 3153.
71 M. Guo and Z.-M. Sun, *J. Mater. Chem.*, 2012, **22**, 15939.
72 D. Tian, Y. Li, R.-Y. Chen, Z. Chang, G. Wang and X. H. Bu, *J. Mater. Chem. A*, 2014, **2**, 1465.

# Supporting Information

## A stable metal-organic framework with suitable pore sizes and rich uncoordinated nitrogen atoms on the internal surface of microspores for highly efficient $CO_2$ capture

Shao-Juan Bao,[a] Rajamani Krishna,[c] Ya-Bing He,[d] Jun-Sheng Qin,[a] Zhong-Min Su,*[a] Shun-Li Li,[a] Wei Xie,[a] Dong-Ying Du,*[a], Wen-Wen He,[a] Shu-Ran Zhang[a] and Ya-Qian Lan*[a,b]

[a] Institute of Functional Material Chemistry, Faculty of Chemistry, Northeast Normal University, Changchun 130024, P. R. China. E-mail: zmsu@nenu.edu.cn

[b] School of Chemistry and Materials Science, Nanjing Normal University, Nanjing 210023, P. R. China. E-mail: yqlan@njnu.edu.cn.

[c] Van't Hoff Institute for Molecular Sciences, University of Amsterdam Science Park 904, 1098 XH Amsterdam (The Netherlands).

[d] College of Chemistry and Life Sciences, Zhejiang Normal University, Jinhua 321004, China.

## S1. Materials and measurements

All the chemicals were obtained from commercial sources, and were used without further purification. Deionized water was used for all experiments. Elemental analyses (C, H and N) were measured on a Perkin-Elmer 2400 CHN elemental analyzer. IR spectrum was performed in the range 4000–400 $cm^{-1}$ using KBr pellets on an Alpha Centaurt FT/IR spectrophotometer. The X-ray powder diffraction (XRPD) data were carried out on a Siemens D5005 diffractometer with Cu-$K_\alpha$ ($\lambda$ = 1.5418 Å). Thermogravimetric analysis (TGA) was recorded on a Perkin-Elmer TG-7 analyzer under nitrogen heated from room temperature to 800 ºC at the heating rate of 5 °C·$min^{-1}$.

### S1.1 Synthesis of NENU-520

A mixture of $H_2L$ (30 mg, 0.11 mmol) and $Zn(NO_3)_2·6H_2O$ (150 mg, 0.50 mmol) was dissolved in a mixture of DMF/EtOH (6 mL/1.5 mL) and droped 0.01 mL $HNO_3$. The mixture was sealed in a 25 mL Teflon-lined autoclave and then heated at 90 °C for 3 days, then cooled to room temperature at 5 °C·$h^{-1}$. Colorless crystals **NENU-520** were collected and washed with DMF for several times (yield 40%, based on $H_2L$). Elemental analysis for $C_{34}H_{30}N_{10}O_6Zn_2$ (805.42): Anal. Calc.: C 50.70; H 3.75; N 17.39. Found: C 50.82; H 3.66; N 17.46%. IR (KBr, $cm^{-1}$): 3430 (w), 1670 (s), 1608 (s), 1571 (s), 1550 (m), 1508 (w), 1459 (m), 1419 (s), 1319 (m), 1255 (w), 1182 (w), 1093 (m), 1006 (w), 840 (m), 788 (s), 768 (s), 680 (w), 523 (w), 424 (w).

### S1.2 X-ray single crystal structure determination

Single crystal X-ray diffraction data in this work were recorded on a Bruker APEXII CCD diffractometer with graphite-monochromated Mo Kα radiation ($\lambda$ = 0.71069 Å) at 293 K. Absorption corrections were applied using multi-scan technique. All the structures were solved by Direct Method of SHELXS-97 and refined by full-matrix least-squares techniques using the SHELXL-97 program within WINGX.[1] Non-hydrogen atoms were refined with anisotropic temperature parameters. The SQUEEZE program implemented in PLATON was used to remove these electron densities for **NENU-520**. Thus, all of electron densities from free solvent molecules have been “squeezed” out.[2] CCDC: 990058 (**NENU-520**) contain the supplementary crystallographic data for this paper. Crystal data are summarized in Table S1 in the Supplementary Information. These data can be obtained free of charge from the Cambridge Crystallographic Data Centre via www.ccdc.cam.ac.uk/data_request/cif.

### S1.3 Gas adsorption experiments

The $N_2$, $H_2$, $CH_4$ and $CO_2$ adsorption measurements were performed on an automatic volumetric adsorption equipment (Quantachrome Autosorb-iQ). Before gas adsorption measurements, the samples were immersed in methanol for 24 h, and the liquid was poured out. Fresh methanol was subsequently added, and the crystals were stay for an additional 24 h to remove the nonvolatile solvates (DMF). The extract was decanted and fresh methanol was added once more. The sample was collected by decanting and treated with dichloromethane similarly to remove methanol solvates. After the removal of dichloromethane by decanting, the sample was activated by drying under a dynamic vacuum at room temperature overnight. Before the measurement, the sample was dried again by using the 'outgas' function of the surface area analyzer for 12 h at room temperature.

### S1.4 Fluorescence study

The finely ground sample **NENU-520** (3 mg) was immersed in 3 mL of different organic solvents. The mixtures were treated by ultrasonication for 30 min, and then aged to form stable suspensions before the fluorescence study. Fluorescence of the samples was performed using a F-4600 FL Spectrophotometer ($\lambda_{ex}$ = 310 nm).

The finely ground sample **NENU-520** (3 mg) was immersed in 3 mL of DMF containing different concentrations of nitrobenzene. The mixtures were treated by ultrasonication for 30 min, and then aged to form stable suspensions before the fluorescence study. Fluorescence of the samples was performed using a F-4600 FL Spectrophotometer ($\lambda_{ex}$ = 310 nm).

## S2. Calculation procedures of selectivity from IAST

### S2.1 Fitting of pure component isotherms

The measured experimental data on e*xcess* loadings, $q^{excess}$, of the pure components $CO_2$, $CH_4$, and $N_2$ in **NENU-520**, were first converted to *absolute* loadings, $q$, using

$$q = q^{excess} + \frac{pV_{pore}}{ZRT} \qquad (1)$$

where $Z$ is the compressibility factor. The Peng-Robinson equation of state was used to estimate $Z$. The accessible pore volume for **NENU-520** is 0.2694 $cm^3/g$.

The isotherm data for $CO_2$, measured at 273 K and 298 K were fitted with the Langmuir-Freundlich model

$$q = q_{sat} \frac{bp^{\nu}}{1 + bp^{\nu}} \quad (2)$$

with $T$-dependent parameter $b$

$$b = b_0 \exp\left(\frac{E}{RT}\right) \quad (3)$$

For $CO_2$, $CH_4$ and $N_2$, the isotherm data at 298 K were fitted with the Langmuir parameters provided in Table S4. Figure S10 provides a comparison of the experimental isotherms in **NENU-520** with the isotherm fits. And the isotherm fits are excellent.

**S2.2 IAST calculations of adsorption selectivities and uptake capacities**

The selectivity of preferential adsorption of component 1 over component 2 in a mixture containing 1 and 2, perhaps in the presence of other components too, can be formally defined as

$$S_{ads} = \frac{q_1/q_2}{p_1/p_2} \quad (4)$$

In equation (4), $q_1$ and $q_2$ are the *absolute* component loadings of the adsorbed phase in the mixture. These component loadings are also termed the uptake capacities. We calculate the values of $q_1$ and $q_2$ using the Ideal Adsorbed Solution Theory (IAST) of Myers and Prausnitz.[3]

**S3. The isosteric heats of adsorption**

The isosteric heat of adsorption, $Q_{st}$, defined as

$$Q_{st} = RT^2 \left(\frac{\partial \ln p}{\partial T}\right)_q \quad (5)$$

were determined using the pure component isotherm fits using the Clausius-Clapeyron equation.

In equation (5), $P$ is pressure, $T$ is temperature, $q$ is the amount adsorbed, $R$ is the gas constant, and $Q_{st}$ denotes the heat of adsorption.

**S4. Transient breakthroughs in fixed bed adsorbers**

The performance of industrial fixed bed adsorbers is dictated by a combination of adsorption selectivity and uptake capacity. For a proper comparison of various MOFs, we perform transient breakthrough simulations using the simulation methodology described in the literature.[4-7] For the breakthrough simulations, the following parameter values were used: length of packed bed, $L$ = 0.3 m; voidage of packed bed,

$\varepsilon$ = 0.4; superficial gas velocity at inlet, $u$ = 0.04 m/s; see schematic in Figure 4. Ther framework density of **NENU-520** is 1318 kg $m^{-3}$.

The transient breakthrough simulation results are presented in terms of a *dimensionless* time, $\tau$, defined by dividing the actual time, $t$, by the characteristic contact time.

## S5. Supporting Figures

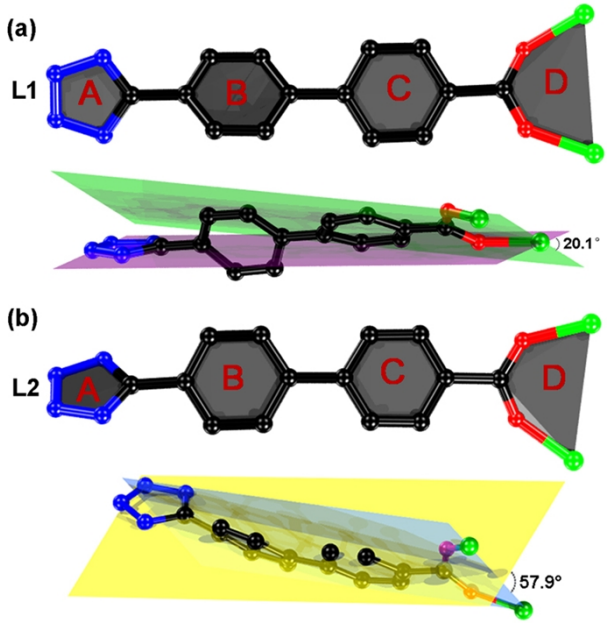


**Fig. S1** The coordination modes of two crystallographically distinct $L^{2-}$ fragments (L1 and L2) in **NENU-520**.

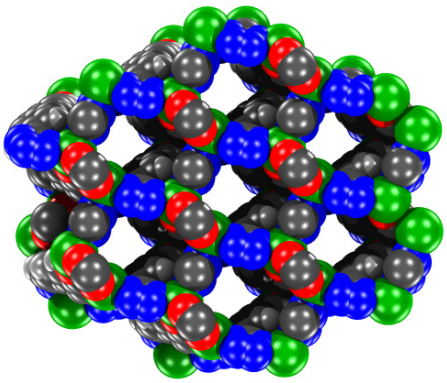

**Fig. S2** The spacefilling representation of the 3D open framework in **NENU-520**.

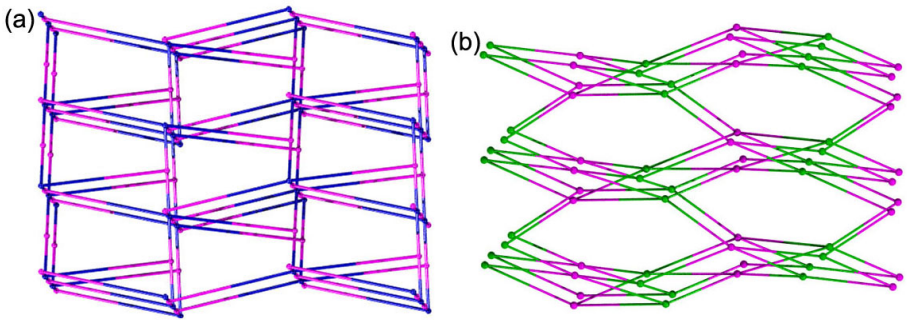


**Fig. S3** The (3,6)-connected (a) and the (4,4)-connected (b) topology net of **NENU-520**.

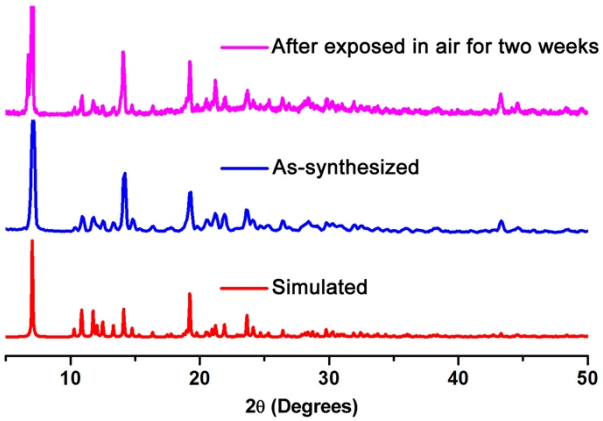


**Fig. S4** The XRPD patterns of **NENU-520**: the stimulated pattern (*red*), the as-synthesized sample (*blue*), and the as-synthesized sample in air for two weeks (*magenta*).

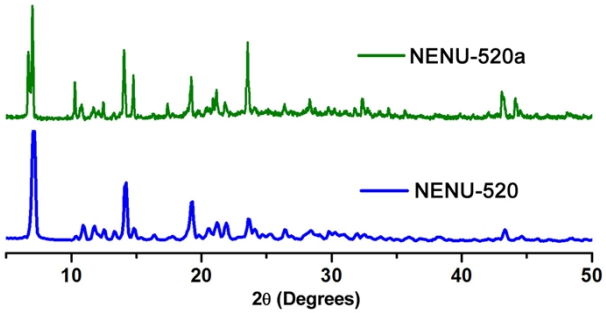


**Fig. S5** The XRPD patterns of the as-synthesized sample **NENU-520** in DMF (*blue*) and the activated sample **NENU-520a** (*green*).

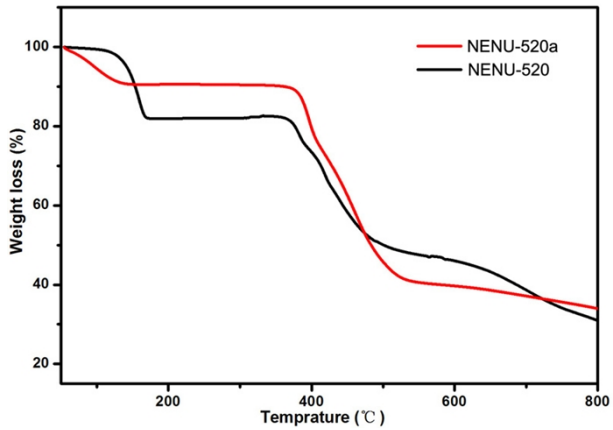


**Fig. S6** The TGA curve of **NENU-520** (*black*) and **NENU-520a** (*red*) measured under $N_2$ atmosphere from room temperature to 800 °C at the heating rate of 5 °C·min$^{-1}$.

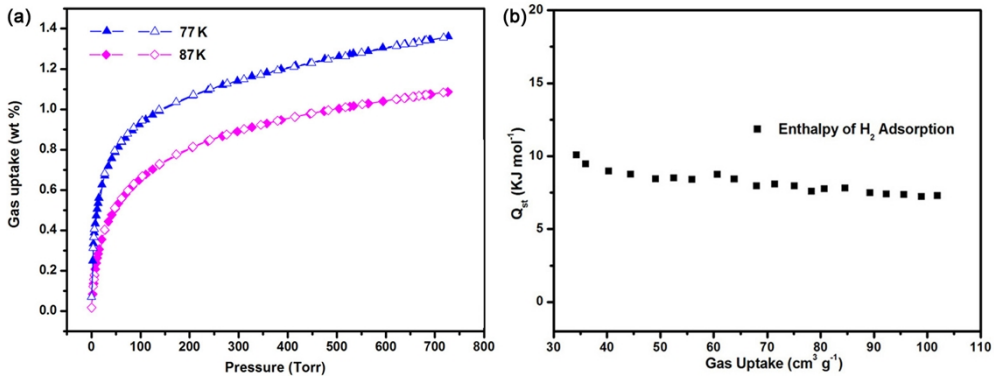


**Fig. S7** (a) $H_2$ sorption isotherms at 77 K (*blue*) and 87 K (*green*) for **NENU-520a**; (b) $Q_{st}$ of $H_2$ calculated by using the Clausius−Clapeyron equation for **NENU-520a**. (solid symbols, adsorption; open symbols, desorption).

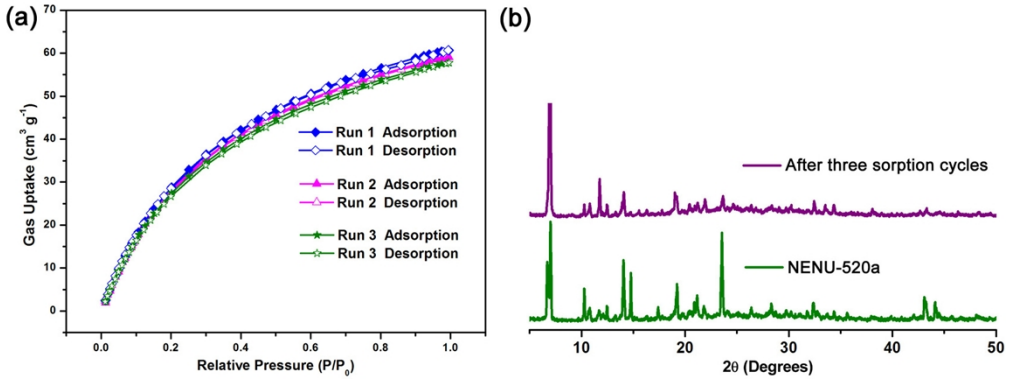


**Fig. S8** (a) The $CO_2$ sorption isotherms at 298 K for **NENU-520a** and (b) the PXRD pattern of the sample after three sorption cycles (*violet*).

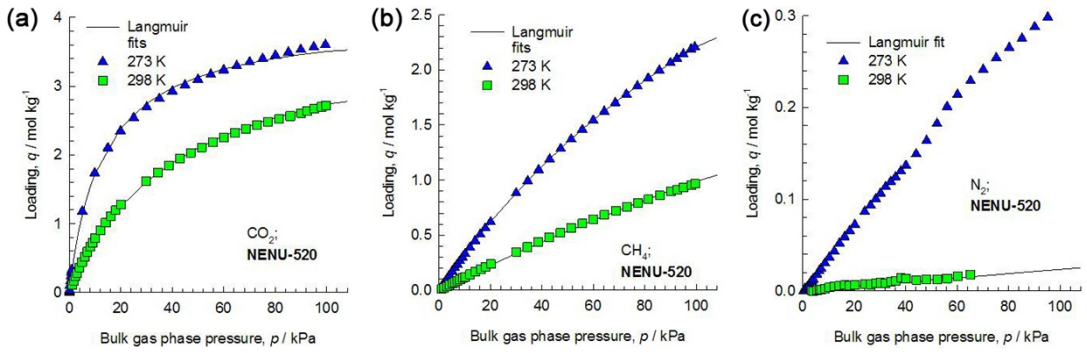


**Fig. S9** Comparison of the pure component isotherm data for (a) $CO_2$, (b) $CH_4$, and (c) $N_2$ in **NENU-520a** with the fitted isotherms (shown by continuous solid lines) at 273 K and 298 K.

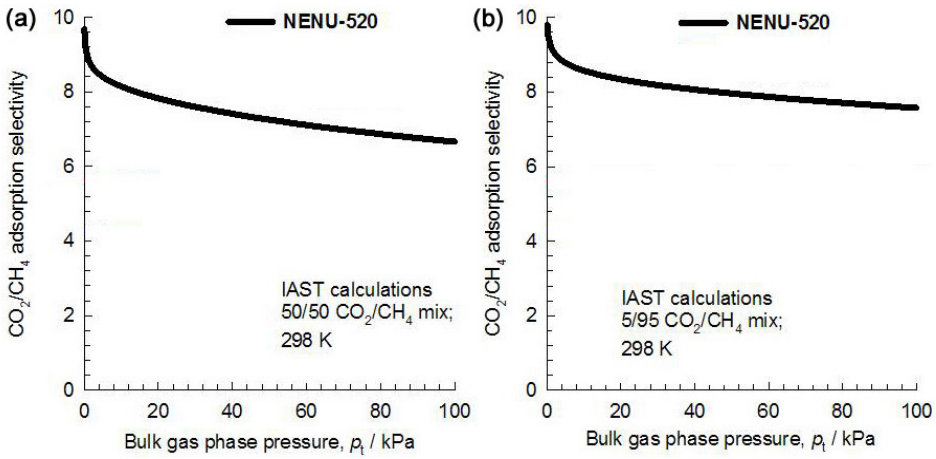


**Fig. S10** Calculations using Ideal Adsorbed Solution Theory (IAST) of Myers and Prausnitz[3] for adsorption selectivitites for (a) 50/50 $CO_2/CH_4$ and (b) 5/95 $CO_2/CH_4$ gas mixtures maintained at isothermal conditions at 298 K in **NENU-520**.

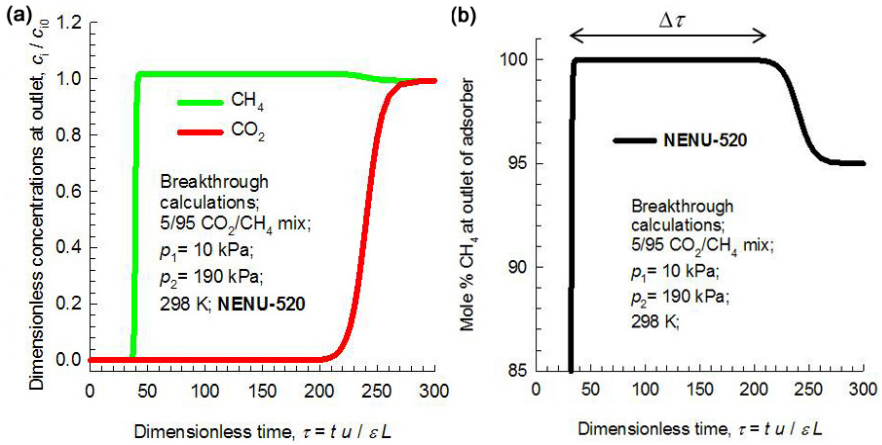


**Fig. S11** Breakthrough characteristics (a) and the mole percent $CH_4$ exiting (b) with 5/95 $CO_2/CH_4$ gas mixtures as a function of the dimensionless time in an adsorber packed with **NENU-520**. These calculations were at 200 kPa total pressure and 298 K.

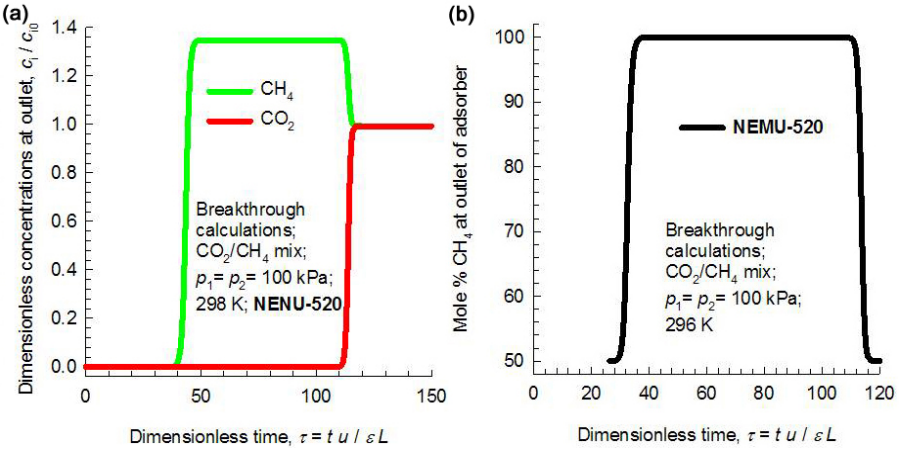

**Fig. S12** Breakthrough characteristics (a) and the mole percent $CH_4$ exiting (b) with 50/50 $CO_2/CH_4$ gas mixtures as a function of the dimensionless time in an adsorber packed with **NENU-520**. These calculations were at 200 kPa total pressure and 298 K.

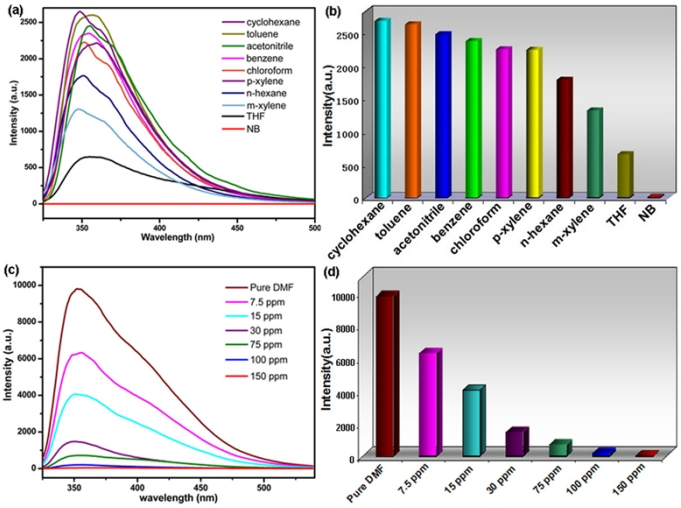


**Fig. S13** (a) and (b) Emission spectra and intensity of **NENU-520** in different organic solvents ($\lambda_{ex}$ = 310 nm, NB = nitrobenzene), (c) and (d) emission spectra and intensity of **NENU-520** in different concentrations of nitrobenzene in DMF ($\lambda_{ex}$ = 310 nm).

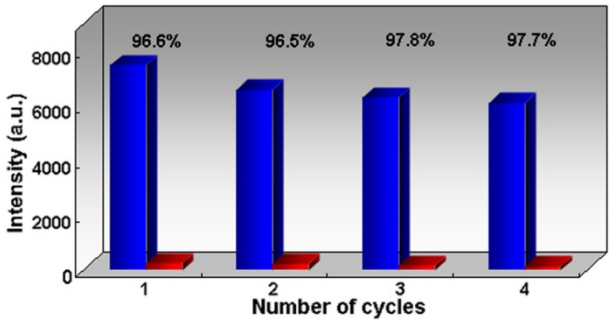


**Fig. S14** Quenching efficiency of **NENU-520** dispersed in DMF to 100 ppm nitrobenzene solution by centrifuging solution after use and washing several times with DMF.

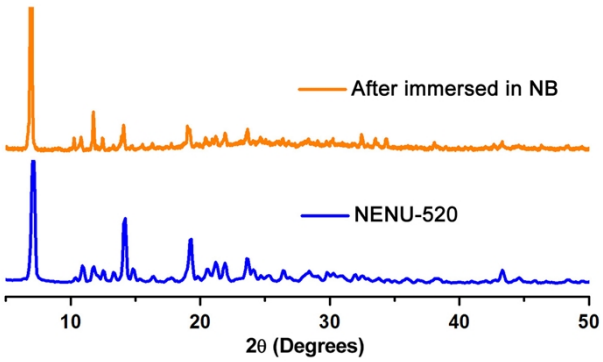


**Fig. S15** The XRPD spectra of **NENU-520**: the as-synthesized samples in DMF (*blue*), and after the detection of nitrobenzene (cycle 4, *orange*), respectively. After every cycle, the samples were centrifuged and washed with DMF for several times.

**Fig. S16** The FT/IR spectra of **NENU-520**: the as-synthesized samples in DMF (*black*), and after the detection of nitrobenzene (cycle 4, *green*). After every cycle, we centrifuged the solution and washed them with DMF for several times.

# S6. Notation

| | |
|---|---|
| $b$ | Langmuir-Freundlich constant for species $i$ at adsorption site A, $Pa^{-\nu_i}$ |
| $c_i$ | molar concentration of species $i$ in gas mixture, mol $m^{-3}$ |
| $c_{i0}$ | molar concentration of species $i$ in gas mixture at inlet to adsorber, mol $m^{-3}$ |
| $E$ | energy parameter, J $mol^{-1}$ |
| $L$ | length of packed bed adsorber, m |
| $p_i$ | partial pressure of species $i$ in mixture, Pa |
| $p_t$ | total system pressure, Pa |
| $q_i$ | component molar loading of species $i$, mol $kg^{-1}$ |
| $Q_{st}$ | isosteric heat of adsorption, J $mol^{-1}$ |
| $t$ | time, s |
| $T$ | absolute temperature, K |
| $u$ | superficial gas velocity in packed bed, m $s^{-1}$ |

## Greek letters

| | |
|---|---|
| $\varepsilon$ | voidage of packed bed, dimensionless |
| $\rho$ | framework density, kg $m^{-3}$ |
| $\nu$ | Freundlich exponent, dimensionless |
| $\tau$ | time, dimensionless |

## S7. Supporting Tables

**Table S1.** Crystal data and structure refinements for **NENU-520**.

| Empirical formula | $C_{34}H_{30}N_{10}O_6Zn_2$ |
|---|---|
| *M*w | 805.42 |
| Crystal system | Monoclinic |
| Space group | *Cc* |
| *a* (Å) | 8.3860(13) |
| *b* (Å) | 17.1990(15) |
| *c* (Å) | 25.132(4) |
| *β* (°) | 94.182(5) |
| *V* (Å$^3$) | 3615.2(9) |
| *Z* | 4 |
| $D_c$ (Mg·m$^{-3}$) | 1.476 |
| Abs.coeff. (mm$^{-1}$) | 1.385 |
| $R_{int}$ | 0.0321 |
| *F*(000) | 1640 |
| reflns collected | 11503 |
| Independent reflns | 6543 |
| GOF on $F^2$ | 1.018 |
| $R_1$[a] | 0.0470 |
| $wR_2$ (all data)[b] | 0.1205 |

[a] $R_1 = \Sigma||F_o| - |F_c||/\Sigma|F_o|$, [b] $wR_2 = |\Sigma w(|F_o|^2 - |F_c|^2)|/\Sigma|w(F_o^2)^2|^{1/2}$.

**Table S2.** The angles between the tetrazole rings and the benzene rings in **NENU-520**.

| Compound | Ligand | Two planes | Dihedral angle/° |
|---|---|---|---|
| **NENU-520** | L1 | AB | 54.8 |
| | | BC | 30.2 |
| | | AD | 20.1 |
| | L2 | AB | 43.6 |
| | | BC | 13.3 |
| | | AD | 57.9 |

**Table S3.** Gas adsorption data of **NENU-520a**.

| Temperature | Gas | Adsorption amount (at saturation) | | | | Number of molecules per unit cell |
|---|---|---|---|---|---|---|
| | | $cm^3\ g^{-1}$ | $cm^3\ cm^{-3}$ | $mmol\ g^{-1}$ | wt % | |
| 77 K | $N_2$ | 151.5 | 199.7 | 6.76 | 18.9 | 19.4 |
| | $H_2$ | 152.4 | 200.9 | 6.80 | 1.36 | 19.5 |
| 87 K | $H_2$ | 121.6 | 160.3 | 5.42 | 1.09 | 15.5 |
| 273 K | $CO_2$ | 80.43 | 106.0 | 3.59 | 15.7 | 10.3 |
| | $CH_4$ | 31.30 | 41.3 | 1.39 | 2.24 | 4.0 |
| | $N_2$ | 6.589 | 8.7 | 0.29 | 0.82 | 0.8 |
| 298 K | $CO_2$ | 60.64 | 79.9 | 2.71 | 11.9 | 7.8 |
| | $CH_4$ | 21.41 | 28.2 | 0.96 | 1.53 | 2.8 |
| | $N_2$ | 0.23 | 0.29 | 0.012 | 0.029 | 0.035 |

**Table S4**. Langmuir-Freundlich parameters for adsorption of $CO_2$, $CH_4$ and $N_2$ at 298 K in **NENU-520**.

| | $q_{sat}$ mol $kg^{-1}$ | $b_0$ $Pa^{-\nu}$ | $\nu$ dimensionless |
|---|---|---|---|
| $CO_2$ | 4 | $7.53\times10^{-11}$ | 0.97 |
| $CH_4$ | 6.2 | $1.56\times10^{-11}$ | 1 |
| N2 | 1 | $2.41\times10^{-7}$ | 1 |

**Table S5.** Comparison of IAST-Calculated Selectivity for $CO_2/CH_4$ and $CO_2/N_2$ Mixture in Different Porous Materials.

| Common names | $CO_2$ capacity | | $CO_2/CH_4$ (Composition and Temperature) | $CO_2/N_2$ (Composition and Temperature) | Reference |
|---|---|---|---|---|---|
| | 273 K | 298 K | 298 K | 298 K | |
| **NENU-520** | **80.43 $cm^3/g$ 106.0 $cm^3/cm^3$ 3.59 mmol/g 15.7 wt%** | **60.64 $cm^3/g$ 79.9 $cm^3/cm^3$ 2.71 mmol/g 11.9 wt%** | **14.1[a] 12.8[b]** | **400[c]** | **In this work** |
| SIFSIX-3-Zn | | 90 $cm^3/cm^3$ | 231[b] | 1818 (10/90) | *Nature,* 2013, **495**, 80-84. |
| Cu(bcppm)$H_2$O | | 1.04 mmol $g^{-1}$ (293 K) | | 590[c] (293K) | *J. Am. Chem. Soc*., 2013, **135**, 10441-10448. |
| UTSA-16 | | 160 $cm^3/cm^3$ (296 K) | | 314.7[c] (296 K) | *Nat Commun,* 2012, ***3,*** 954-963 |
| MAF-66 | 140 $cm^3/g$ | 99 $cm^3/g$ | 5.8 | 225[b] | *Inorg. Chem*., 2012, **51**, 9950−9955. |
| $[Cu(tba)_2]_n$ | 51.8 $cm^3/g$ | 43.9 $cm^3/g$ | 45[c] (293 K, 1 bar) | 45[c] (293 K, 1 bar) | *J. Am. Chem. Soc*., 2014, ***136***, 10906-10909. |
| [Zn(btz)]·DMF·0.5$H_2O$ | 98 $cm^3/g$ | | | | *J. Am. Chem. Soc*., 2012, **134**, 784- 787. |
| P5-SOF | | 8.8 wt% | 375 | 339 | *Adv. Mater*., DOI: 10.1002/adma.201401672. |
| Zn(HL)·$H_2O$]·DMA | 0.93 mmol g-1 | | | | *Chem. Commum.,* 2014, **50**, 6886-6889. |
| MAF-23 | 74.2 $cm^3/g$ | 56.1 $cm^3/g$ | | 107[d] | *J. Am. Chem. Soc*., 2012, **134**, 17380-17383. |
| PCP-1 | 56.5 g $L^{-1}$ | | | | *Chem. Sci.*, 2014, **5**, 660-666 |
| $Zn_2(atz)_2(oba)$ | 80.6 $cm^3/g$ | 55.2 $cm^3/g$ | | | *Cryst. Growth Des*., 2013, **13**, 2118-2123. |
| mmen-CuBTTri | | 4.2 mmol/g | | 327 | *Energy Environ. Sci*., 2011, **4**, 3030-3040. |
| $Mg_2$(dobpdc) | | 6.42 mmol/g | | 200 | *J. Am. Chem. Soc*., 2012, ***134***, 7056-7065. |
| CALF-32 ($BF_4$) | 1.5 mmol $g^{-1}$ | | | | *Inorg. Chem. Front*., 2014, **1,** 302-305. |
| BILP-11 | 5.06 mmol $g^{-1}$ | | 7.6 | 56 (0.05 bar) | *J. Mater. Chem. A*, 2014, **2**, 12492-12500. |
| $[Co_2(pbdc)_2(bimb)_2(bimb)_{0.5}$ | 48.8 | 28.2 $cm^3/g$ | 5 | 19 | *J. Mater. Chem. A*, 2014, **2**, 12413-12422. |
| NOP-20 | 11.8 wt% | 7.2 wt% | | | *J. Mater. Chem. A*, 2014, **2**, 7795 - 7801. |
| ZIF-300 | | 40 $cm^3/cm^{-3}$ | | 22[b] | *Angew. Chem. Int. Ed*., 2014, **53**, 1-5. |

[a] Selectivity of $CO_2$ over $CH_4$ or $N_2$ when the gas phase mole fractions is 5/95;

[b] Selectivity of $CO_2$ over $CH_4$ $N_2$ when the gas phase mole fractions is 50/50;

[c] Selectivity of $CO_2$ over $N_2$ predicted when the gas phase mole fractions is 15/85;

[d] Calculated from pure component isotherms by Henry's law.

## References


1 (a) G. M. Sheldrick, SHELXS-97, Programs for X-ray Crystal Structure Solution, University of Göttingen, Göttingen, Germany, 1997; (b) G. M. Sheldrick, SHELXL-97, Programs for X-ray Crystal Structure Refinement, University of Göttingen, Göttingen, Germany, 1997; (c) L. J. Farrugia, WINGX, A Windows Program for Crystal Structure Analysis, University of Glasgow; Glasgow, UK, 1988.

2 A. L. Spek, *J. Appl. Crystallogr*., 2003, **36**, 7.

3 A. L. Myers and J. M. Prausnitz, *AIChE J.*, 1965, **11**, 121.

4 R. Krishna and J. R. Long, *J. Phys. Chem. C*, 2011, ***115***, 12941.

5 R. Krishna, *Microporous Mesoporous Mater.* 2014, ***185***, 30.

6 D. L Chen, H. Shang, W. Zhu and R. Krishna, *Chem. Eng. Sci.,* 2014, ***117***, 407.

7 D. L. Chen, N. Wang, F. F.Wang, J. Xie, Y. Zhong, W. Zhu, J. K. Johnson, and R. Krishna, *J. Phys. Chem. C*, 2014, ***118***, 17831.